Rev. Roum. Sci. Techn.– Électrotechn. et Énerg.
Vol. **71**, *4*, pp. 483–488, Bucarest, 2026

HESSIAN-FREE FLUX OPTIMIZATION FOR ENERGY-EFFICIENT INDUCTION MOTOR DRIVES: EXPERIMENTAL VALIDATION

NGOC THUY PHAM [1]

Keywords: Induction motor drives; Hessian-free Optimization; Field-oriented control; Efficiency optimization.

Conventional field-oriented control (FOC) of induction motor drives typically employs a fixed flux reference, leading to reduced energy efficiency, particularly under light-load conditions due to excessive excitation and increased losses. To address this limitation, this paper proposes a lightweight Hessian-free adaptive flux optimization strategy. A simple real-time update law for the d-axis current is developed, enabling effective loss minimization without requiring second-order derivative computation, iterative optimization, or additional hardware. By capturing the nonlinear coupling between torque demand and excitation, the method dynamically adjusts the flux while preserving the conventional FOC structure. Experimental results demonstrate significant efficiency improvement over a wide operating range, with efficiency increasing from 31.02% to 61.87% under light-load conditions and from 69.07% to 77.61% at rated load compared to conventional PI-based FOC. The proposed approach provides a low-complexity solution suitable for real-time industrial applications.

1. INTRODUCTION

Induction motor (IM) drives are widely used in industrial and energy conversion systems due to their ruggedness, cost-effectiveness, and high reliability [1–3]. Field-oriented control (FOC) is the standard approach owing to its ability to decouple torque and flux dynamics, ensuring satisfactory transient and steady-state performance [3-5]. However, conventional FOC employs a fixed flux reference, neglecting its dependence on load and speed. This results in excessive excitation under light-load conditions, leading to increased copper and core losses and reduced efficiency [6,7].

To address this issue, various efficiency-oriented strategies have been developed. Model-based methods such as loss-model control (LMC), optimal flux regulation, and maximum torque per ampere (MTPA) determine optimal excitation by minimizing analytical loss functions [8–12]. However, their performance depends on accurate motor parameters, which are affected by temperature, saturation, and aging, thereby reducing robustness [13,14]. In addition, the associated nonlinear optimization problems often require iterative solutions, leading to high computational burden and limited real-time applicability [15,16].

Predictive control methods, including MPC and PTC, integrate efficiency optimization into a unified framework [17,18]. While offering flexibility, their implementation is constrained by high computational complexity and sensitivity to model inaccuracies [19–23]. Observer-based techniques improve robustness but often involve complex design and may exhibit stability issues in nonlinear or low-speed regions [10,13]. Data-driven approaches, such as neural networks and deep learning, can model nonlinear dynamics but typically require large datasets, incur high computational cost, and lack interpretability [24].

From an industrial perspective, a gap remains between advanced optimization techniques and practical deployment. Existing methods often rely on high computational resources, precise parameter identification, or complex implementation, limiting their applicability in real-time systems [25–29]. Therefore, there is a need for lightweight approaches that enhance efficiency while preserving the simplicity and robustness of conventional FOC.

To address this challenge, this paper proposes a lightweight Hessian-free adaptive flux optimization strategy for IM drives. A simple real-time update law for the d-axis current is developed, enabling loss minimization without explicit second-order derivatives, iterative computation, or additional hardware. By capturing the coupling between torque demand, speed, and excitation, the method adaptively adjusts the flux to improve efficiency over a wide operating range while maintaining the conventional FOC structure. Compared with existing approaches, it reduces computational complexity and is suitable for real-time implementation. Experimental results verify consistent efficiency improvement over a wide operating range, highlighting the suitability of the proposed method for real-time industrial applications.

The main contributions are as follows:

(1) A lightweight Hessian-free flux optimization strategy for efficiency improvement.

(2) A real-time update law for the d-axis current while preserving the FOC structure.

(3) Experimental validation demonstrating significant efficiency improvement, particularly under light-load conditions, without degrading dynamic performance.

The remainder of the paper is organized as follows. Section 2 presents the IM model, Section 3 describes the Hessian-free optimization method, Section 4 provides experimental validation, and Section 5 concludes the paper.

2. MATHEMATICAL DESCRIPTION OF IMDS

The state-space model of the IM drive is given as follows:

$$\dot{\mathbf{x}}(t)=\mathbf{A}\mathbf{x}(t)+\mathbf{B}\mathbf{u}(t). \tag{1}$$

where **x**, **A**, **B**, and **u** can be defined as:

$$\mathbf{x}(t)=[i_{s\alpha}\quad i_{s\beta}\quad \psi_{r\alpha}\quad \psi_{r\beta}\quad \omega_r]^{\mathrm{T}}.$$

$$\mathbf{u}(t)=[u_{s\alpha}\quad u_{s\beta}\quad T_L]^{\mathrm{T}}.$$

$$\mathbf{A}=\begin{bmatrix} a_{11} & 0 & a_{13} & a_{14} & a_{15} \\ 0 & a_{11} & -a_{14} & a_{13} & a_{25} \\ \frac{L_m}{\tau_r} & 0 & \frac{-1}{\tau_r} & \omega_r & \psi_{r\beta} \\ 0 & \frac{L_m}{\tau_r} & -\omega_r & \frac{-1}{\tau_r} & -\psi_{r\alpha} \\ -b\psi_{r\beta} & b\psi_{r\alpha} & bi_{s\beta} & -bi_{s\alpha} & \left(\frac{-b}{J}\right) \end{bmatrix}, \mathbf{B}=\begin{bmatrix} \frac{1}{\sigma L_s} & 0 & 0 \\ 0 & \frac{1}{\sigma L_s} & 0 \\ 0 & 0 & 0 \\ 0 & 0 & 0 \\ 0 & 0 & \frac{-1}{\mathrm{J}} \end{bmatrix}.$$

$$\tau_r=\frac{L_r}{R_r};\sigma=1-\frac{L_m^2}{L_rL_s};\gamma=\frac{L_m}{L_r};k=\frac{3pL_m}{2L_r};b=\frac{k}{J};$$

[1] Faculty of Electrical Engineering Technology, Industrial University of Ho Chi Minh City, Vietnam.
E-mail: phamthuyngoc@iuh.edu.vn

DOI: 10.59277/RRST-EE.2026.4.4

$$a_{11} = -\frac{1}{\sigma L_s}\left(R_s + \frac{L_m^2}{L_r \tau_r}\right), a_{13} = \frac{\gamma}{\sigma L_s \tau_r}, a_{14} = -\frac{\gamma}{\sigma L_s}\omega_r,$$

$$a_{15} = -\frac{\gamma}{\sigma L_s}\psi_{r\beta};\ a_{25} = \frac{\gamma}{\sigma L_s}\psi_{r\alpha}, \quad (2)$$

where $i_{s\alpha,\beta}, u_{s\alpha,\beta}, \psi_{r\alpha,\beta}$ are components of the stator's current, stator's voltage, and rotor's flux in the αβ reference frame. T_L is the load torque; L_s, L_r, L_m are the stator, rotor, and mutual inductances; R_s, R_r are the stator and rotor resistances; J is the inertia of the motor; σ is the total linkage coefficient; p is the number of pole pairs; τ_r is the rotor time constant; ω_r is the rotor speed. The electromagnetic torque and mechanical dynamics follow,

$$T_e = \frac{3}{2} p \frac{L_m}{L_r} \psi_{rd} i_{sq}, \quad (3)$$

$$J\frac{\mathrm{d}\omega_r}{\mathrm{d}t} = T_e - T_L - B\omega_r. \quad (4)$$

3. HESSIAN-FREE LOSS MINIMIZATION CONTROL DESIGN

In IM drives, energy efficiency is governed by the nonlinear interaction between copper losses and core losses, which are directly dependent on the current distribution in the dq reference frame. Under steady-state operating conditions, the total power loss can be expressed:

$$P_{loss} = R_s\left(i_{sd}^2 + i_{sq}^2\right) + R_r i_{sq}^2 + k_{fe}\varphi_s^2\omega_e. \quad (5)$$

where k_{fe} is the core loss coefficient and ω_e is the electrical angular speed. Under the FOC framework, the stator flux is approximated linearly as $\varphi_s = L_m i_{sd}$, which allows the loss function to be fully expressed:

$$P_{loss}\left(i_{sd}, i_{sq}\right) = R_s\left(i_{sd}^2 + i_{sq}^2\right) + R_r i_{sq}^2 + k_{fe}L_m^2 i_{sd}^2\omega_e. \quad (6)$$

By incorporating the torque constraint:

$$T_e = \frac{3p}{2} L_m i_{sd} i_{sq}, \quad (7)$$

the torque-producing current can be expressed as:

$$i_{sq} = \frac{2T_e}{3pL_m i_{sd}}. \quad (8)$$

Substituting into the loss expression yields a single-variable nonlinear optimization problem:

$$P_{loss}(i_{sd}) = R_s i_{sd}^2 + (R_s + R_r)\left(\frac{2T_e}{3pL_m i_{sd}}\right)^2 + k_{fe}L_m^2 i_{sd}^2\omega_e. \quad (9)$$

The function $P_{loss}(i_{sd})$ exhibits a convex-like structure over the feasible domain $i_{sd} > 0$, as it consists of quadratic and inverse quadratic terms. Therefore, there exists at least one global minimum corresponding to the optimal flux level for each operating condition (T_e, ω_e).

The derivative of the loss function with respect to i_{sd} reveals the nonlinear and curvature characteristics of the problem:

$$\frac{\mathrm{d}P_{loss}(i_{sd})}{\mathrm{d}i_{sd}} = 2R_s i_{sd} - 2(R_s + R_r)\frac{4T_e^2}{(3pL_m)^2 i_{sd}^3} + 2k_{fe}L_m^2 i_{sd}. \quad (10)$$

From a theoretical standpoint, the optimal point can be obtained by solving this equation. However, real-time implementation is not feasible due to the strong nonlinearity and continuous variation of T_e and ω_e. This leads to a fundamental requirement: an optimization strategy that is both fast, stable, and sufficiently accurate for real-time tracking of the optimal point. First-order methods such as gradient descent are simple but fail to exploit curvature information, resulting in slow convergence and strong dependence on step-size tuning. In contrast, classical second-order methods such as Newton's method achieve faster convergence but require explicit Hessian computation and matrix inversion, which are impractical for embedded systems due to high computational complexity and sensitivity to parameter uncertainties, so a Hessian-free (HF) optimization strategy is adopted. Instead of explicitly computing the Hessian matrix, the method utilizes Hessian-vector products:

$$H\delta = -g, \quad (11)$$

$$g_k = \nabla P_{loss}\left(i_{sd}(k)\right). \quad (12)$$

The Hessian-vector product is approximated using directional derivatives:

$$Hv \approx \frac{\nabla P(i_{sd} + \varepsilon\upsilon) - \nabla P(i_{sd})}{\varepsilon}. \quad (13)$$

This approach eliminates the explicit computation of second-order derivatives, preserving the fast convergence of second-order methods. The resulting subproblem is efficiently solved using the conjugate gradient method to obtain the optimal search direction with low computational complexity. Based on this direction, the flux-producing current is updated as:

$$i_{sd}^{opt}(k+1) = i_{sd}(k) + \alpha\delta_k. \quad (14)$$

This formulation enables continuous adaptive flux control, allowing the system to track the minimum-loss trajectory without solving a full optimization problem at each time step. Importantly, the optimization process only modifies the reference value i_{sd}, while the conventional FOC structure remains unchanged, ensuring seamless integration into existing systems.

Theorem 1 (existence and uniqueness of optimal flux): For $T_e > 0$, $\omega_e > 0$, the loss function:

$$P_{loss}(i_{sd}) = a i_{sd}^2 + \frac{b}{i_{sd}^2}, \quad (15)$$

$$a = R_s + k_{fe}L_m^2\omega_e;\ b = (R_s + R_r)\left(\frac{2T_e}{3pL_m}\right)^2$$

Strictly convex for $i_{sd} > 0$, yielding a unique global minimizer i_{sd}^*.

Proof:

$$\frac{\mathrm{d}P_{loss}}{\mathrm{d}i_{sd}^2} = 2a + \frac{6b}{i_{sd}^4} > 0. \quad (16)$$

The optimal solution is given by:

$$i_{sd}^* = \left(\frac{b}{a}\right)^{1/4}. \quad (17)$$

Theorem 2 (descent property of the HF update law) Consider the update law:

$$i_{sd}(k+1) = i_{sd}(k) + \alpha\delta_k, \quad (18)$$

where δ_k is obtained from the Hessian-free system:

$$H\delta_k = -g_k, \quad (19)$$

with $g_k = \nabla P_{loss}(i_{sd}(k))$. Then, there exists a sufficiently small $\alpha > 0$ such that:

$$P_{loss}(k+1) < P_{loss}(k). \tag{20}$$

Proof: Since δ_k is an approximate solution of:

$$\min\left(\frac{1}{2}\delta^{\mathrm{T}} H\delta + g_k^{\mathrm{T}}\delta\right), \tag{21}$$

it follows that: $g_k^{\mathrm{T}}\delta < 0$

The conjugate gradient iterations are performed:

$$\begin{aligned} &\delta_{k+1} = \delta_k + \alpha_k p_k;\ \alpha_k = \frac{r_k^{\mathrm{T}} r_k}{p_k^T H p_k}, \\ &r_k = H\delta_k + g;\ \beta_k = \frac{r_{k+1}^{\mathrm{T}} r_{k+1}}{r_k^T r_k};\ p_{k+1} = -r_{k+1} + \beta_k p_k. \end{aligned} \tag{22}$$

Using first-order Taylor expansion:

$$P_{loss}(k+1) \approx P_{loss}(k) + \alpha g_k^{\mathrm{T}}\delta_k. \tag{23}$$

Since $g_k^{\mathrm{T}}\delta_k < 0, \exists\alpha > 0$, such that $P_{loss}(k+1) < P_{loss}(k)$

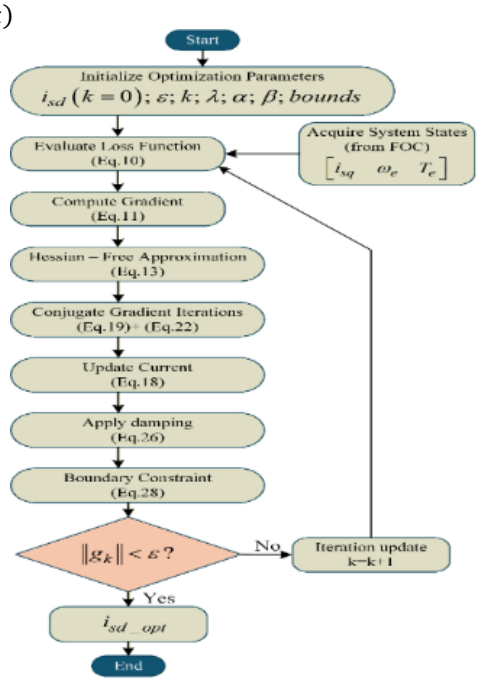


Fig. 1 – Flowchart of the Hessian-free loss minimization algorithm.

Theorem 3 (local convergence of HF flux adaptation)

Assume that the gradient ∇P_{loss} is Lipschitz continuous in a neighborhood of i_{sd}^*, and the approximated Hessian H is positive definite. Then, the sequence $i_{sd}(k)$ generated by the HF update law converges locally to the optimal solution i_{sd}^*

Proof: Since $P_{loss}(i_{sd})$ is strictly convex and twice differentiable, there exists a Lipschitz constant L such that:

$$\|\nabla P(\mathbf{x}) - \nabla P(\mathbf{y})\| \le L\|\mathbf{x} - \mathbf{y}\|. \tag{24}$$

From Theorem 2, it follows that:

$$P_{loss}(k+1) \le P_{loss}(k) - c\|g_k\|^2, \tag{25}$$

with $c > 0$. This ensures that the sequence $P_{loss}(k)$ is monotonically decreasing and bounded below by P_{loss}^*. According to standard convergence results for descent methods with Lipschitz gradients:

$$\lim_{k\to\infty} g_k = 0 \Rightarrow i_{sd}(k) \to i_{sd}^*. \tag{26}$$

Thus, local convergence is guaranteed.

To ensure stability and practical feasibility, the Hessian operator is regularized as:

$$\mathbf{H}' = \mathbf{H} + \lambda\mathbf{I}, \tag{27}$$

and the optimized current is constrained within allowable limits.

The implementation of the proposed Hessian-free loss minimization strategy is illustrated in Fig. 1. Compared with first-order methods, it yields more efficient search directions while retaining a lightweight structure suitable for real-time motor drives. Derived from the analytical loss model, the approach enables continuous adaptation of excitation, allowing operation near the minimum-loss region over a wide load range and improving efficiency, particularly under light-load conditions, without altering the conventional FOC framework.

4. RESULTS AND DISCUSSION

To evaluate the proposed Hessian-free (HF) flux optimization strategy, real-time experiments are conducted on a squirrel-cage induction motor with the parameters as follows: P = 1/4 HP, U = 220 V, f = 50 Hz, J = 0.0003 kg·m^2, p = 2, R_s = 9.8 Ω, R_r = 9.6 Ω, L_s = 0.311 H, L_r = 0.3112 H, L_m = 0.29 H. The overall drive system (Fig. 2) adopts a conventional FOC structure augmented with the proposed HF-based loss minimization mechanism, with the control architecture and experimental setup shown in Figs. 3 and 4, respectively. Experimental data are acquired via the Monitor & Tune interface in MATLAB/Simulink, enabling real-time observation of speed, torque, and current responses.

4.1 PERFORMANCE ANALYSIS UNDER RATED LOAD DISTURBANCES

The experimental results under rated load conditions, summarized in Table 1 and illustrated in Fig. 5, reveal a consistent improvement in energy efficiency achieved by the proposed HF-based flux optimization strategy across the entire speed range.

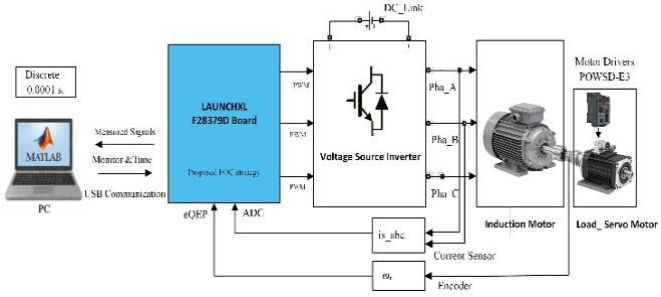


Fig. 2 – Experimental setup of the FOC-based IM drive system

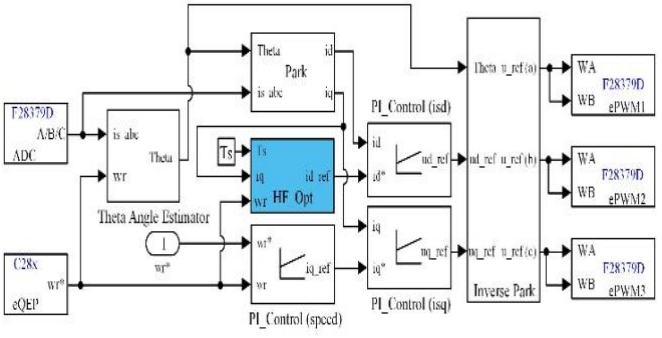
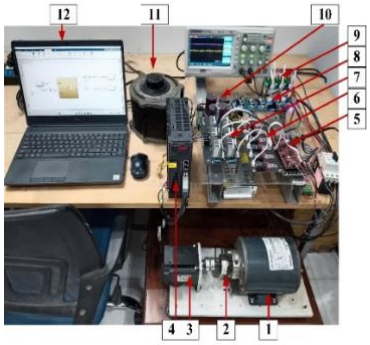


Fig. 3 – Proposed FOC scheme implemented in real time on a DSP platform (TI F28379D).



1) IM
2) Encoder
3) Servomotor (Load)
4) Servodrive
5) Texas Instruments TMS320F28379D
6) IGBT drive;
7) Voltage source inverter;
8) Voltage sensor;
9) Current sensor;
10) DC-link voltage;
11) AC variac power
12) Host PC

Fig. 4 – Experimental setup of the IM drive.

At high speed (110 rad/s), the efficiency increases from 69.07% to 77.61%, accompanied by a reduction in power loss from 9.50 W to 7.53 W. While the absolute reduction appears moderate, it reflects a more efficient allocation of current components, where the excitation level is adjusted to avoid excessive core losses without compromising torque production. A similar trend is observed at 85 rad/s, where the loss reduction (from 9.26 W to 7.03 W) is accompanied by a significant efficiency gain, indicating that the proposed method effectively adapts the flux level to the operating point. More importantly, at low speed (25 rad/s), the efficiency improvement becomes significantly more pronounced, increasing from 38.15% to 57.19%. This behavior reveals a key characteristic of the proposed method: under low-speed operation, conventional PI-based FOC tends to maintain a non-optimal excitation level, resulting in disproportionately high losses relative to the output power. In contrast, the HF-based strategy dynamically adjusts the flux according to the loss curvature, achieving a more balanced trade-off between torque and flux currents. This observation is consistent with the theoretical formulation in Section 3, where the optimal flux is obtained by minimizing the combined effect of copper and core losses. Even under rated load conditions, the proposed method can accurately track this optimal operating point, leading to measurable efficiency gains.

Table 1

Efficiency comparison under 100% rated load at different speeds.

Speed (rad/s)	PI			HF-Opt		
	Efficiency (%)	Power loss (W)	Energy loss (J)	Efficiency (%)	Power loss (W)	Energy loss (J)
110	69.07	9.50	332.62	77.61	7.53	263.66
85	64.12	9.26	324.00	75.41	7.03	246.05
25	38.15	7.66	268.23	57.19	5.61	196.29

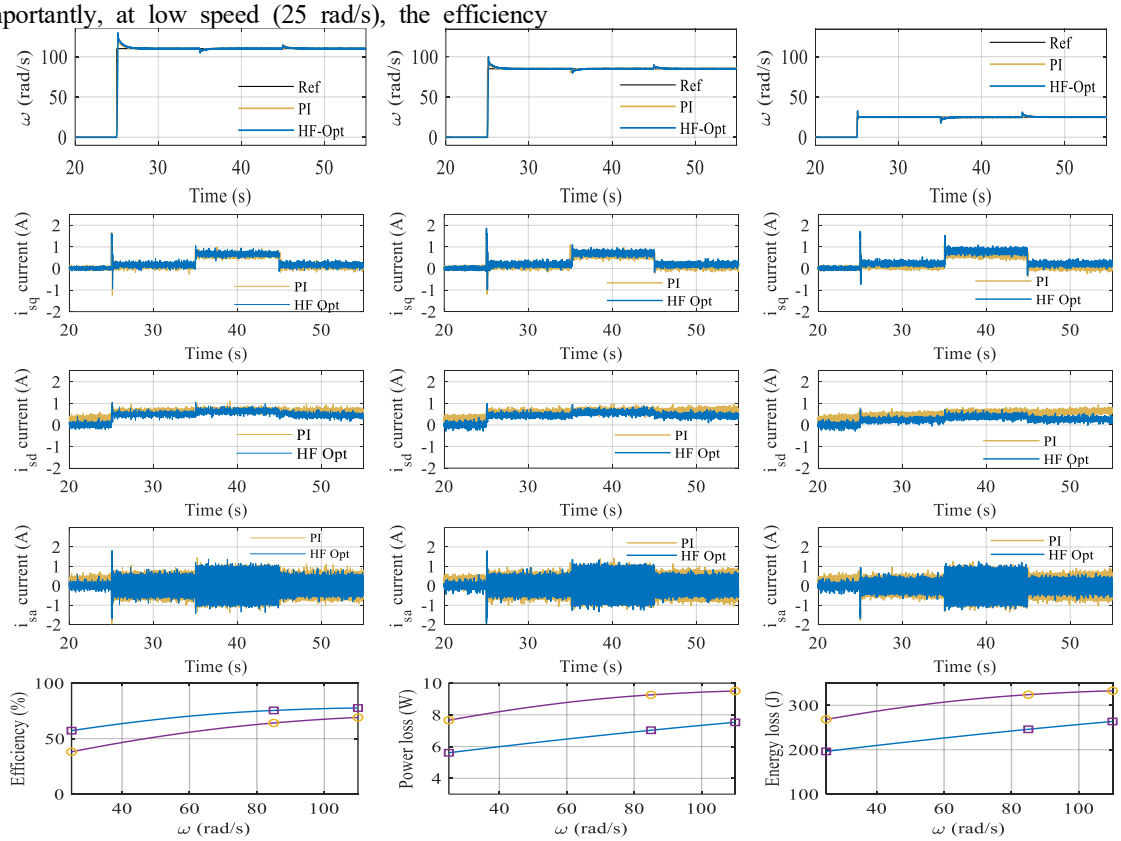


Fig. 5 – Efficiency response under rated load at different speed levels (PI (purple); HF Opt (light blue).

4.2 PERFORMANCE ANALYSIS UNDER PARTIAL-LOAD CONDITIONS

The effectiveness of the proposed method becomes most evident under partial-load conditions of operation (50 % rated load), as shown in Fig. 6 and Table 2. In this regime, conventional PI-based FOC operates with a nearly constant magnetizing current that depends weakly on load torque, leading to excessive excitation and increased copper losses. Specifically, at high speed (110 rad/s), the efficiency improves from 58.89% (PI) to 76.47%, while the power loss decreases from 9.35 W to 5.74 W. This indicates that a significant portion of the losses under PI control originates from overestimated excitation, which is effectively mitigated by the proposed optimization. A similar trend is observed at 85 rad/s, where the efficiency increases from 57.04% to 75.69%, and the power loss reduces from 7.56 W to 5.09 W, confirming that the proposed method maintains accurate flux adaptation across varying operating points.

The improvement becomes most pronounced at low speed (25 rad/s), where the efficiency increases from 31.02% to 61.87%, accompanied by a reduction in power loss from 6.16 W

to 3.61 W. This behavior reflects the severe mismatch between torque demand and fixed excitation in conventional FOC under part-load conditions. In contrast, the proposed method adjusts the excitation current according to the loss gradient, thereby reducing unnecessary magnetization and shifting the operating point toward the minimum of the loss function. These results are fully consistent with the theoretical formulation in Section 3, where the optimal excitation is obtained by minimizing the total loss function. The improvement is therefore most significant under part-load conditions, particularly at low speeds, where total losses are most sensitive to excitation current.

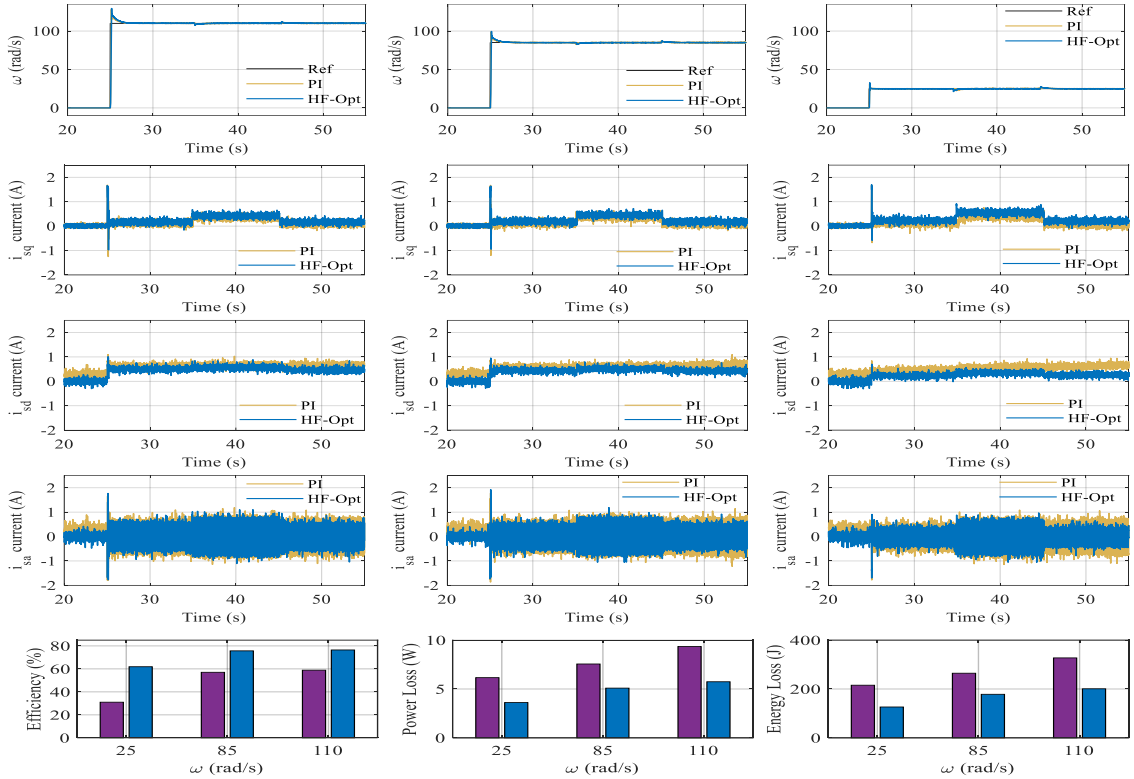


Fig. 6 - Efficiency response under light-load conditions (50% rated load) at different speed levels (PI (purple); HF Opt. (light blue).

Table 2

Efficiency comparison under light-load conditions (50% rated load) at different speeds

Speed (rad/s)	PI			HF-Opt		
	Efficiency (%)	Power loss (W)	Energy loss (J)	Efficiency (%)	Power loss (W)	Energy loss (J)
110	58.89	9.35	327.33	76.47	5.74	200.80
85	57.04	7.56	264.63	75.69	5.09	178.32
25	31.02	6.16	215.52	61.87	3.61	126.31

4.3 PERFORMANCE ANALYSIS AND DISCUSSION

The overall impact of the proposed HF-based optimization strategy is further illustrated in Figs. 7(a)- 7(b), which provide a global view of the efficiency and loss characteristics over a wide range of operating conditions.

It can be observed that the operating points obtained with the proposed method are consistently shifted toward regions associated with lower power and energy losses compared to the conventional PI-based control. More importantly, this shift is not uniform across the operating space. The deviation becomes increasingly pronounced in the low-load region, where the loss surfaces exhibit higher sensitivity with respect to *isd.* This indicates that the conventional PI-based FOC operates with an overestimated excitation current, leading to a systematic bias away from the minimum-loss trajectory.

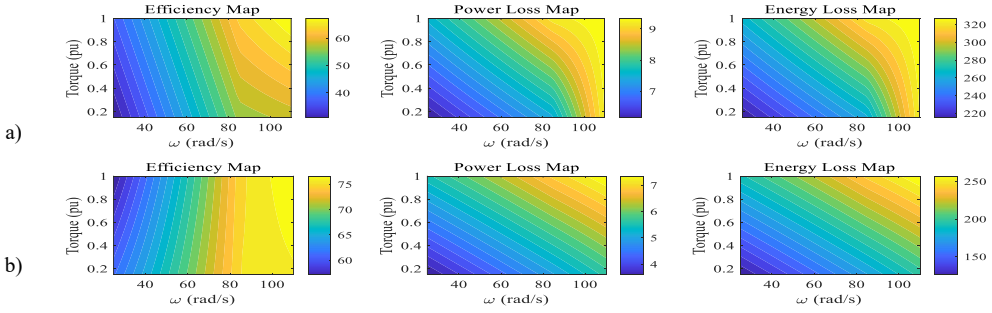


Fig. 7 - Efficiency, power loss, and energy loss maps of the induction motor under different operating conditions. (a) Conventional PI-based FOC control. (b) PI-based FOC with the proposed HF-based i_{isdref} optimization.

From a control perspective, this behavior reflects the ability of the proposed HF-based strategy to exploit the local curvature of the loss function $P_{loss}(i_{sd})$ to determine the optimal i_{sdref} in real time. As a result, the operating point is continuously projected toward the minimum of the loss surface without requiring explicit Hessian computation. In contrast to heuristic or search-based methods, the proposed approach provides a structured and computationally efficient update mechanism derived directly

from the analytical form of the loss function. Importantly, these improvements are achieved without modifying the fundamental structure of the FOC scheme. The optimization is introduced as a supervisory layer that generates the optimal i_{sdref}, while the inner current control loops remain unchanged. This separation of roles ensures implementation simplicity and preserves the robustness of the underlying control structure, making the proposed method well suited for practical drive systems, particularly in applications dominated by partial-load operation.

5. CONCLUSIONS

This paper presents a Hessian-free optimization strategy to enhance the energy efficiency of induction motor drives within the conventional FOC framework. By formulating the loss minimization problem in terms of the d-axis current, a simple real-time update law is developed without explicit Hessian computation, iterative optimization, or additional hardware. The proposed method continuously adapts the excitation current according to operating conditions, thereby reducing unnecessary losses caused by excessive flux in conventional PI-based FOC. Theoretical analysis verifies the existence and uniqueness of the optimal solution, together with the descent and local convergence properties of the update law. Experimental validation on a real-time test bench demonstrates significant efficiency improvement over a wide operating range, especially under partial-load conditions. These improvements are achieved without modifying the original FOC structure, enabling straightforward integration into existing industrial drive systems while preserving control dynamics. Compared with existing efficiency-oriented methods, the proposed approach offers lower computational complexity and simpler implementation while maintaining consistent efficiency gains. By performing optimization directly in the control variable space, the method avoids the complexity and sensitivity of model-based and predictive approaches. Future work will extend the framework to address parameter variations, magnetic saturation, multi-objective optimization, and applications to other electric drives.

CREDIT AUTHORSHIP CONTRIBUTION STATEMENT

Ngoc Thuy PHAM: Conceptualization, methodology, controller design, analysis, simulation, real-time implementation, data curation, validation, investigation, writing original draft, writing—review and editing.

Received on 11 April 2026

REFERENCES

1. J. Holtz, “Sensorless control of induction motor drives”, Proc. IEEE, **90**, *8*, pp. 1359–1394 (2002).
2. I.M. Mehedi, N. Saad, M.A. Magzoub, U.M. Al-Saggaf, A.H. Milyani, “Simulation analysis and experimental evaluation of improved field-oriented controlled induction motors incorporating intelligent controllers”, IEEE Access, **10**, pp. 18380–18394 (2022).
3. M.G. Simões, “A concise history of induction motor drives—Part 1”, IEEE Electrification Magazine, **11**, *2*, pp. 5–11 (2023).
4. T. Orłowska-Kowalska, M. Korzonek, G. Tarchała, “Stability improvement methods of the adaptive full-order observer for sensorless induction motor drive—Comparative study”, IEEE Trans. Ind. Inform., **15**, *11*, pp. 6114–6126 (2019).
5. N.T. Pham, “A hybrid intelligent control framework with real-time validation for induction motor drives”, Rev. Roum. Sci. Techn. – Électrotechn. Et Énerg., **71**, *1*, pp. 45–52 (2026).
6. A.M. Bazzi, P.T. Krein, "Review of methods for real-time loss minimization in induction machines”, IEEE Trans. Ind. Appl., **46**, pp. 2319–2328 (2010).
7. Z. Qu, M. Ranta, M. Hinkkanen, J. Luomi, “Loss-minimizing flux level control of induction motor drives”, IEEE Trans. Ind. Appl., **48**, *3*, pp. 952–961 (2012).
8. M. Abdelwanis, R. El-Sehiemy, “Efficient parameter estimation procedure using sunflower optimization algorithm for six-phase induction motor”, Rev. Roum. Sci. Techn. – Électrotechn. Et Énerg., **67**, *3*, pp. 259–264 (2022).
9. R. Sivaraju, R. Dhanabal, P. Kumar, P. Vijayakumar, K. Jayakumar, “Improving the efficiency of induction motor drive by flux and torque control: A hybrid LSE-RERNN approach”, ISA Transactions, **147**, pp. 215–226 (2024).
10. L. Wogi, M. Morawiec, T. Ayana, P. Kołodziejek, “Multiscalar control-based flux optimization for efficiency improvement of induction motor”, IEEE Trans. Transp. Electrific., **11**, *6*, pp. 14047–14061 (2025).
11. A. De Keyser, H. Vansompel, G. Crevecoeur, “Real-time energy-efficient actuation of induction motor drives using approximate dynamic programming”, IEEE Trans. Ind. Electron., **68**, *12*, pp. 11837–11846 (2021).
12. R. Basak, A.K. Paul, “Cost-effective design of three-phase induction motor: An optimization approach”, Rev. Roum. Sci. Techn. – Électrotechn. Et Énerg., **67**, *4*, pp. 461–466 (2022).
13. M.S. Mousavi, S. Rezaei, A. Khayati, H. Oraee, “Predictive torque control of induction motor based on a robust integral sliding mode observer”, IEEE Trans. Ind. Electron., **70**, *3*, pp. 2339–2350 (2023).
14. Y. Zhang, Z. Yin, R. Tang, J. Liu, “Moment of inertia and load torque identification based on adaptive extended Kalman filter for interior permanent magnet synchronous motors”, IEEE Trans. Instrum. Meas., **74**, pp. 1–12 (2025).
15. Y. El.-G. Boudissa, M. Bounekhla, F. Habbi, “Enhanced spiral dynamic algorithm with application to induction motor parameters identification”, Rev. Roum. Sci. Techn. – Électrotechn. Et Énerg., **70**, *4*, pp. 441–448 (2026).
16. I. Sami, S. Ullah, A. Basit, N. Ullah, J. Ro, “Integral super twisting sliding mode based sensorless predictive torque control of induction motor”, IEEE Access, **8**, pp. 186740–186755 (2020).
17. J. Martens, “Deep learning via Hessian-free optimization”, Proc. Int. Conf. Mach. Learn., pp. 735–742 (2010).
18. Y. Zhang, Y. Bai, H. Yang, B. Zhang, “Low switching frequency model predictive control of three-level inverter-fed IM drives with speed-sensorless and field-weakening operations”, IEEE Trans. Ind. Electron., **66**, *6*, pp. 4262–4272 (2019).
19. Y. Zhang, L. Shao, Z. Yin, C. Bai, J. Liu, “Ultralocal model-based model predictive torque control of induction motor drives with model-free speed controller”, IEEE Trans. Ind. Electron., **72**, *9*, pp. 8962–8973 (2025).
20. N.I. Nahin, M.S. Kaiser, M.T. Arif, S. Shama, R. Ahmed, “Predictive torque control with reduced voltage vectors for voltage source inverter-driven induction motor drives”, IEEE Trans. Appl. Supercond., **34**, *8*, pp. 1–5 (2024).
21. W. Xu, Y. Tang, D. Dong, X. Xiao, E.E.M. Rashad, A.K. Junejo, “Optimal reference primary flux-based model predictive control of linear induction machine with MTPA and field-weakening operations for urban transit”, IEEE Trans. Ind. Appl., **58**, *4*, pp. 4708–4721 (2022).
22. Y. Gong, X. Zhao, L. Wang, “Improved robust model predictive current control via high-order terminal sliding mode control for permanent magnet synchronous motor”, IEEE Trans. Autom. Sci. Eng., **23**, pp. 5237–5249 (2026).
23. I.D. De Martin, F. Tinazzi, M. Zigliotto, “Tuning-less model predictive torque control for synchronous motor drives with maximum torque-per-ampere criterion including transients”, IEEE Trans. Power Electron., **40**, *9*, pp. 12393–12401 (2025).
24. S. Zhang, R. Chen, W. Du, Y. Yuan, V.S. Vassiliadis, “Neural speed torque estimator for induction motors in the presence of measurement noise”, IEEE Trans. Ind. Electron., **70**, *1*, pp. 167–177 (2023).
25. X. Guo, Q. Yang, Q. Wang, Y. Sun, A. Tan, “Electromagnetic torque modeling and validation for a permanent magnet spherical motor based on XGBoost”, Simulation Modeling Practice and Theory, **136**, article 102989 (2024).
26. N. Ali, W. Alam, M. Pervaiz, J. Iqbal, “Nonlinear adaptive backstepping control of permanent magnet synchronous motor," Rev. Roum. Sci. Techn. – Électrotechn. Et Énerg., **66**, *1*, pp. 9–14 (2021).
27. S. Zhang, R. Chen, W. Du, Y. Yuan, V.S. Vassiliadis, “A Hessian-free gradient flow method for the optimisation of deep learning neural networks”, Comput. Chem. Eng., **141**, article 107008 (2020).
28. Z.-D. Zhou, G. Guo, R. Zhang, “Hessian-free fixed-/predefined-time algorithms for distributed time-varying optimization”, IEEE Trans. Syst., Man, Cybern.: Syst., **55**, *10*, pp. 6890–6900 (2025).
29. Y. He, P. Gong, Z. Lu, “Efficiency optimization strategy of induction motor based on electromagnetic and reactive torque control”, IEEE Trans. Transp. Electrific., **11**, *6*, pp. 13815–13825 (2025).